

Heating by an Electron Bernstein Wave in a Spherical Tokamak Plasma via Mode Conversion

S. Shiraiwa,^{1,*} K. Hanada,² M. Hasegawa,² H. Idei,² H. Kasahara,¹ O. Mitarai,³ K. Nakamura,² N. Nishino,⁴ H. Nozato,⁵ M. Sakamoto,² K. Sasaki,⁶ K. Sato,² Y. Takase,¹ T. Yamada,⁷ H. Zushi,² and TST-2@K Group

¹Graduate School of Frontier Sciences, University of Tokyo, Kashiwa 277-8561, Japan

²Research Institute for Applied Mechanics, Kyushu University, Kasuga 816-8580, Japan

³Institute of Industrial Science and Technical Research, Kyushu Tokai University, Kumamoto 862-8652, Japan

⁴Graduate School of Engineering, Hiroshima University, Higashi-Hiroshima 739-8527, Japan

⁵Graduate School of Engineering, Osaka University, Suita 565-0871, Japan

⁶Graduate School of Engineering Sciences, Kyushu University, Kasuga 816-8580, Japan

⁷Graduate School of Science, University of Tokyo, Bunkyo 113-0033, Japan

(Received 18 January 2006; published 12 May 2006)

The first successful high power heating of a high dielectric constant spherical tokamak plasma by an electron Bernstein wave (EBW) is reported. An EBW was excited by mode conversion (MC) of an X mode cyclotron wave injected from the low magnetic field side of the TST-2 spherical tokamak. Evidence of electron heating was observed as increases in the stored energy and soft x-ray emission. The increased emission was concentrated in the plasma core region. A heating efficiency of over 50% was achieved, when the density gradient in the MC region was sufficiently steep.

DOI: 10.1103/PhysRevLett.96.185003

PACS numbers: 52.50.Sw, 52.55.Fa

The spherical tokamak (ST) is a tokamak with an extremely low aspect ratio (R/a , where R is the major radius and a is the minor radius). Compared to conventional tokamaks and stellarators, ST has the advantage of achieving stable high β (the ratio of plasma pressure to magnetic pressure) plasmas, which is considered an attractive property for an economically competitive fusion reactor. Since ST plasmas are generally highly overdense ($\omega_{pe}^2/\omega_{ce}^2 = 10\text{--}100$, where ω_{pe} and ω_{ce} are electron plasma and cyclotron angular frequencies, respectively), their dielectric properties are rather different from conventional tokamak and stellarator plasmas. Hence, the development of new plasma heating techniques using radio-frequency (rf) waves is required. In the MHz frequency range, heating by the high harmonic fast wave was demonstrated in the National Spherical Torus experiment [1]. In the GHz frequency range, both the lower hybrid and the electron cyclotron waves, commonly used in underdense plasmas, have poor accessibility to the core of overdense plasmas and are considered to be inefficient for heating and current drive. An electron Bernstein wave (EBW), which has no density cutoff and is efficiently absorbed by electron cyclotron damping, has been proposed as a promising candidate for heating and current drive in overdense plasmas.

Since an EBW is a short wavelength electrostatic wave and is difficult to excite directly, mode conversion (MC) from longer wavelength electromagnetic modes (O mode or X mode) is used. Two MC scenarios have been proposed and demonstrated on fusion plasmas with $\omega_{pe}^2/\omega_{ce}^2 \sim 1$. Heating and current drive by the high magnetic field side X mode launch (X - B) MC has been demonstrated in conventional tokamaks [2,3]. The second MC scenario (O - X - B) was first demonstrated on the Wendelstein 7-AS stellarator [4,5]. However, the X - B scenario from the high-field side is not usable in ST plasmas because of the

existence of the left-hand cutoff on the high-field side (see the locations of the two cutoff layers in Fig. 1) and the O - X - B scenario is more difficult in ST since the magnetic field geometry is not determined by external coils alone. The third possibility, employed in this experiment,

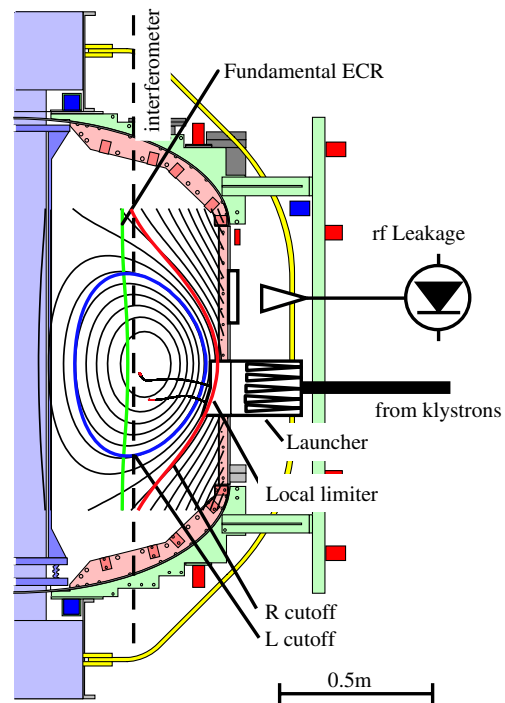


FIG. 1 (color online). Cross-sectional view of TST-2@K. Typical equilibrium flux surfaces and the locations of critical layers are shown. The rf leakage monitor is installed 120° away toroidally from the launcher. Fundamental ECR (electron cyclotron resonance) is located slightly at the high field side of the magnetic axis.

uses the low-field side X mode launch [6,7]. Although this scenario has the advantage of simple launcher design, the required density gradient in the MC region is steeper than that occurring naturally in ST plasmas. It was reported that the radiation temperature (T_{rad}) of EBW emission from the CDX-U spherical tokamak plasma could be enhanced to the level of $T_{\text{rad}} \sim T_e$ by inserting a local limiter around the receiving antenna [8]. A more complicated technique to improve the MC efficiency has also been proposed. In Ref. [9], it is shown that by controlling the polarization, one can enhance the MC efficiency over a wide range of magnetic field and density gradient at the MC layer, though a complicated hardware design is required. This Letter reports the results of the first high power heating experiment in highly overdense plasmas ($\omega_{pe}^2/\omega_{ce}^2 \sim 10$) carried out on the Tokyo Spherical Tokamak 2 (TST-2) device [10], using the low-field side incidence X - B MC scenario.

The experimental setup is shown in Fig. 1. TST-2 is a small ST constructed at the University of Tokyo with nominal major radius $R = 0.38$ m, minor radius $a = 0.25$ m, toroidal magnetic field at major radius $B_t = 0.3$ T, and plasma current $I_p = 0.14$ MA. For this set of experiments, TST-2 was temporarily moved to Kyushu University (TST-2@K), where high power microwave sources (200 kW at 8.2 GHz) were available. Microwave power was injected through eight horn antennas located on the low-field side of the torus. The antenna array was surrounded by a CDX-U-like local limiter made of molybdenum. The local limiter could be moved from -15 to 25 mm relative to the fixed low-field side limiter located at $R = 0.64$ m, where the negative direction is defined to be in the direction approaching the plasma. Langmuir probes were installed inside the local limiter to measure the density profile. The rf leakage monitor was used as an indicator of the power that goes neither to the plasma nor back to the launcher.

In Fig. 1, typical equilibrium flux surfaces and the locations of the critical layers are shown. It is noted that both the left-hand and right-hand cutoff layers exist in a very narrow region on the low-field side and that an upper hybrid resonance layer (not shown) exists between them. The existence of the cutoff on the high density side changes the MC efficiency drastically from the case of a linear and singular turning point doublet, considered by Budden [11]. The calculated MC efficiency for the present experimental condition (8.2 GHz and 0.18 T) is shown in Fig. 2. A resonant absorption model using the cold plasma dielectric tensor is used in the calculation, which gives the MC efficiency with acceptable accuracy when finite temperature effects can be neglected. Over 80% MC is achievable when a rather short density scale length of ~ 5 mm is realized. Typical ray trajectories calculated by a ray-tracing code are also shown in Fig. 1. The code calculates the trajectory of the EBW generated at the edge MC layer until 99% of the wave power is absorbed. The wave power is absorbed by electrons in the plasma core region by

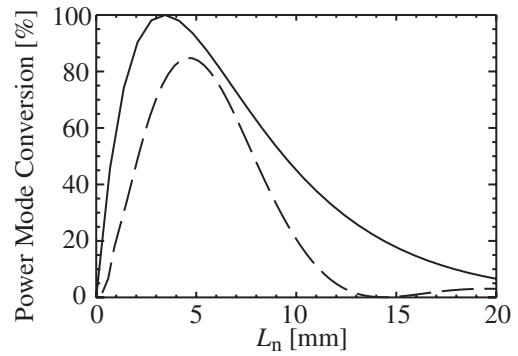


FIG. 2. Calculated MC efficiency for X - B mode conversion as a function of density scale length ($L_n \equiv n/|dn/dx|$). The solid line is C_{max} defined in [6].

fundamental cyclotron damping. We observed good antenna-plasma coupling for various local limiter locations, and up to 140 kW of the net rf power was injected successfully.

Figure 3 shows a plasma discharge in which a significant increase of the plasma stored energy was observed. The net rf power was 70 kW in this discharge. An outboard limited plasma with a plasma current of about 100 kA was maintained for several milliseconds. The line-averaged density (\bar{n}_e), defined as the line-integrated density divided by the path length of the interferometer chord through the plasma, was $1 \times 10^{19} \text{ m}^{-3}$ at rf turn-on, which is an order of magnitude above the cutoff density. At rf turn-on, a clear increase of the plasma stored energy (W_K) by 15%–20% was observed as shown in Fig. 3(c). Since the power input

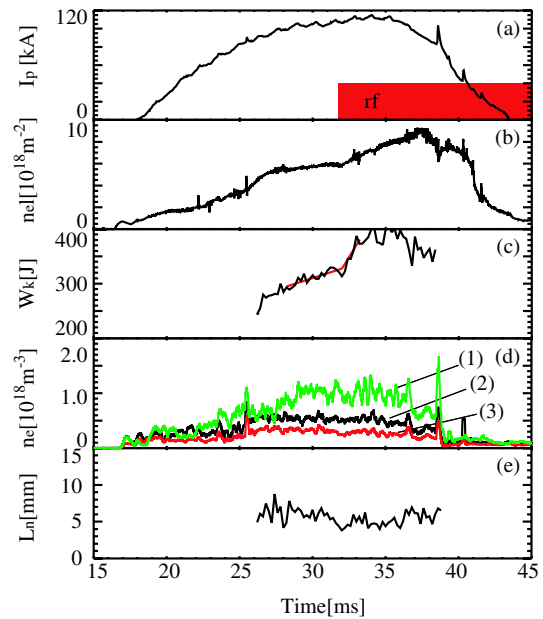


FIG. 3 (color online). Plasma discharge with 70 kW of net rf power (#301462). (a) Plasma current, (b) line-integrated density $\bar{n}_e l$ at $R = 0.38$ m ($l \approx 0.6$ m), (c) plasma stored energy, (d) densities measured at three locations inside the local limiter, and (e) density scale length.

from Ohmic heating is 300 kW on average from 30 to 35 ms, the increase of W_K corresponds to 45–60 kW of additional heating, assuming no degradation of energy confinement with power. The absorbed power can also be estimated from a break-in-slope analysis, which indicates that the heating power increased by 35–45 kW at rf turn-on. In addition, W_K saturated after about 1 ms after rf turn-on. This time scale is similar to the energy confinement time. An increase of the line-averaged density was also observed, suggesting an increased particle source. However, the time scale of the density increase is much longer than that of W_K and cannot be considered as the main cause of W_K increase. These results consistently indicate that the rf power heated the plasma with over 50% efficiency.

The electron densities measured by Langmuir probes are shown in Fig. 3(d). Probe (1), which is closest to the plasma, is not completely shadowed by the local limiter, while probes (2) and (3) are completely shadowed by the local limiter. An electron temperature of 30 eV was obtained in a similar discharge by sweeping the voltage applied to probe (1) and this temperature was used to calculate the electron density from the ion saturation current (I_s). The density scale length L_n inside the local limiter is shown in Fig. 3(e). The measured L_n was about 6 mm. Noting that the scale length naturally created outside the local limiter was about 30 mm, the local limiter indeed shortened L_n and 70%–80% MC is expected from Fig. 2. Assuming the same T_e for all three probes introduces an uncertainty in the estimation of L_n . However, even if the temperature scale length (L_{T_e}) were assumed to be equal to L_n , L_n would be only 1.5 times larger than L_{T_e} and 30%–40% MC is still expected. The observed increase of W_K is consistent with L_n between these two cases.

An indication of high energy electron generation was also observed. In the discharge shown in Fig. 4, rf power was injected into a target plasma with approximately 30% lower line-averaged density ($\bar{n}_e \sim 0.7 \times 10^{19} \text{ m}^{-3}$). A more complete set of diagnostics was operating. Shown in the figure are $n_e l$, H_α emission, radiated power P_{rad} (measured by an absolute extreme ultraviolet detector), and soft x-ray (SX, 1–10 keV) emission measured by a surface barrier diode with a beryllium filter and the plasma stored energy W_K , all of which increased at rf turn-on. The increase of SX emission indicates that high energy electrons are generated by EBW injection at the beginning of rf injection. However, a direct electron temperature measurement was not available (a previous measurement of T_e using x-ray pulse height analysis in plasmas with 100 kA plasma current was 400 eV). During the rf pulse, SX turned over, while P_{rad} continued to increase, suggesting that the loss of heating may be caused by increased radiation. A step-function-like response observed in H_α emission (0.6 ms rise time) indicates that some power is deposited directly in the plasma edge. The timing of the stored energy turnover was approximately the same as the SX signal turnover, indicating that heating is effective while high energy electrons are generated.

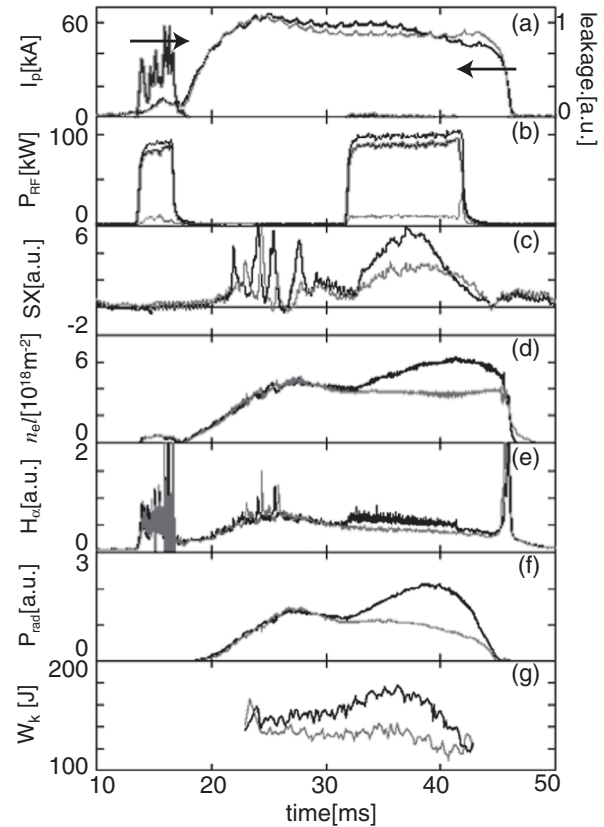


FIG. 4. Time evolutions of discharges with 90 kW net rf injection (#302787 in black) and without rf power (#302788 in gray). (a) Plasma current and rf leakage power, (b) forward, reflected, and net rf powers, (c) SX (1–10 keV) emission, (d) line-integrated density at $R = 0.38 \text{ m}$ ($l \approx 0.55 \text{ m}$), (e) H_α , (f) P_{rad} (broadband radiation over the range 0.01–7 keV), and (g) plasma stored energy.

Figure 5 shows the evolution of the SX emission profile for the #302787 discharge shown in Fig. 4. The emission was measured by a 20-channel positive-intrinsic-negative (PIN) diode array, viewing the plasma from the low-field side. A clear increase of the emission from the core region after rf turn-on can be seen in Fig. 5. The movement of the intensity peak towards lower channels after 37 ms is consistent with the motion of the magnetic axis calculated by equilibrium reconstruction. Figure 5(b) shows the evolution of the peak intensity of the SX profile. Two other PIN diode arrays of the same type, viewing the plasma from the top and the bottom of the torus, respectively, also showed significant increases of the signal only in the channels viewing the plasma core region. Hence, the emission increase is localized in the plasma core region ($r/a \leq 0.4$) where an EBW is expected to be absorbed via the cyclotron damping.

The heating efficiency was lower in the discharge shown in Fig. 4 (W_K increased from 150 to 170 J, by 13%). This can be explained by considering the effect of the shallow density gradient region outside the local limiter. Figure 6 shows the MC efficiency calculated using a model density

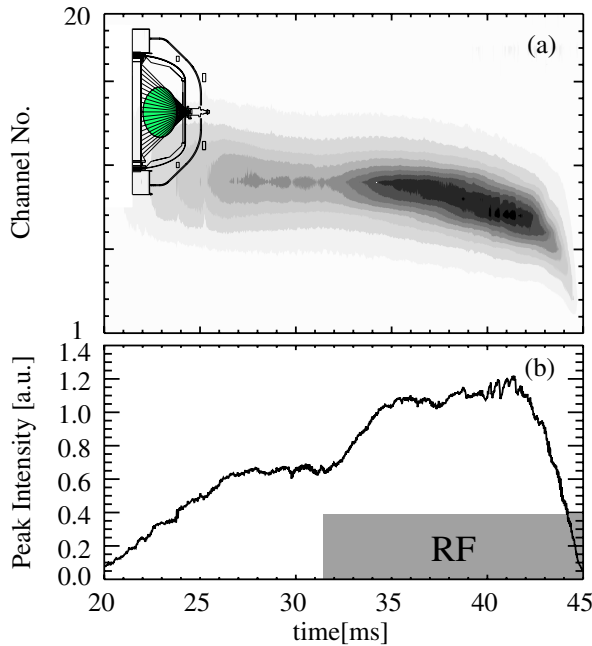


FIG. 5 (color online). (a) Contour plot of PIN diode array signals, and (b) evolution of the peak intensity.

profile, with L_n inside the local limiter ($L_{n\text{-limiter}}$) chosen to be the optimum for MC and L_n outside the local limiter chosen to be $5 \times L_{n\text{-limiter}}$. When the density at the front edge of the local limiter (limiter edge density, n_{edge}) is high enough so that the cutoff-resonance-cutoff triplet is located well inside the local limiter, the efficiency shown in Fig. 2 is reproduced. As n_{edge} decreases, the efficiency decreases. This is because the high density cutoff moves outside the local limiter and the triplet becomes stretched radially (note that the high density cutoff for 8.2 GHz at 0.18 T is $1.3 \times 10^{18} \text{ m}^{-3}$). The narrow peak at $n_{\text{edge}} \sim 0.6 \times 10^{18} \text{ m}^{-3}$ is caused by the resonance of the wave reflected by the two cutoff layers. The experimentally observed heating efficiencies including the two discharges discussed above are overplotted in Fig. 6. In a real plasma, edge density fluctuations are expected to smear out the fine structure shown in Fig. 6, so the observed dependence of the heating efficiency on density is plausible. (In a discharge with similar $n_e l$ to #302787, it was confirmed that n_{edge} was about 70% of #301462.)

A remaining question is where the power goes in the lower density case with poor core absorption. The rf leakage monitor indicates that the rf power was absorbed somewhere inside the vacuum vessel and the H_α signal response indicates that some power is absorbed in the plasma edge region directly. The increased density may change the trajectory of the EBW and move the rf power deposition layer towards the plasma edge, where confinement is poor. According to ray tracing, the shift is calculated to be $\Delta r/a \leq 0.1$ and the deposition remains in the plasma core region, even if the density increased by a factor of 3. Calculations show that collisional damping

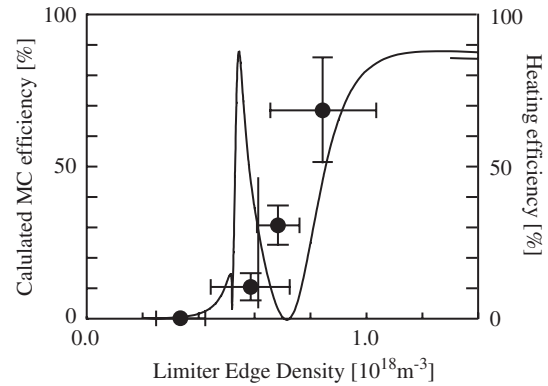


FIG. 6. Comparison between calculated MC efficiency for a density profile consisting of steep (shallow) gradient regions [inside (outside) the local limiter] and the observed heating efficiency. The upper and lower bounds of the measured limiter edge density are based on the measured density at probe (1) and the density extrapolated to the limiter edge from probe (2).

during a single pass through the plasma edge is not significant. However, multiple reflections between the plasma and the vacuum vessel wall may enhance edge absorption by this process significantly.

In this Letter, results of the first EBW heating experiments based on the low-field side incidence X - B MC scenario are reported. A heating efficiency of over 50% was observed. The increase of SX emission indicated generation of high energy electrons. The emission profile measured by three PIN diode arrays confirmed absorption in the plasma core region. The heating efficiency became poorer in a lower density discharge, in which the triplet is not completely inside the local limiter. These results demonstrate that the X - B MC scenario from the low-field side can be used successfully for plasma heating.

This work was supported by joint-use research RIAM Kyushu University and JSPS Grant-in-Aid for Scientific Research.

*Present address: 1-36-2-308, Hakusan, Bunkyo-ku, Tokyo 113-0001, Japan.

Electronic address: shiraiwa@i-love-anemone.com

- [1] J.R. Wilson *et al.*, Phys. Plasmas **10**, 1733 (2003).
- [2] V. Shevchenko *et al.*, Phys. Rev. Lett. **89**, 265005 (2002).
- [3] T. Maekawa *et al.*, Phys. Rev. Lett. **86**, 3783 (2001).
- [4] H. P. Laqua *et al.*, Phys. Rev. Lett. **90**, 075003 (2003).
- [5] H. P. Laqua *et al.*, Phys. Rev. Lett. **81**, 2060 (1998).
- [6] A.K. Ram and S.D. Schultz, Phys. Plasmas **7**, 4084 (2000).
- [7] P.C. Efthimion *et al.*, Rev. Sci. Instrum. **70**, 1018 (1999).
- [8] B. Jones *et al.*, Phys. Rev. Lett. **90**, 165001 (2003).
- [9] H. Igami *et al.*, Plasma Phys. Controlled Fusion **46**, 261 (2004).
- [10] Y. Takase *et al.*, Nucl. Fusion **41**, 1543 (2001).
- [11] K.G. Budden, *Radio Waves in the Ionosphere* (Cambridge University Press, Cambridge, England, 1966).